CHEMO-MECHANICAL EFFECTS ON ROCK STRENGTH, YOUNG'S MODULUS AND POISSON'S RATIO

by

Joshua Caine Thompson

A thesis submitted to the faculty of
The University of Utah
in partial fulfillment of the requirements for the degree of

Master of Science

Department of Chemical Engineering

The University of Utah

December 2010

The University of Utah Graduate School

STATEMENT OF THESIS APPROVAL

The thesis of **Joshua Caine** [redacted]

has been approved by the following supervisory committee members

[redacted]

and by [redacted], Chair of

the Department of **Chemical** [redacted]

and by Charles A. Wight, Dean of The Graduate School

ABSTRACT

The effect of fluids on rock strength, Young's Modulus and Poisson's Ratio is complicated and not well understood. However, many applications involving rock-fluid interactions are of considerable interest, and often pose significant physical and economic impact on a given project. Experimental measurements were carried out to assess the role of various fluids on Young's modulus, Poisson's ratio and strength of three rock types—Indiana limestone, Salt Wash South and Berea Buff sandstone. The alteration of mechanical properties as a function of fluid and exposure time was evaluated. Oven-dried, deionized water saturation, salt brine saturation, and odorless mineral spirits (OMS) saturation were assessed using unconfined compression testing. A number of triaxial compression tests at high confining pressures were also conducted. In all cases, drained conditions were maintained.

Results are provided, showing substantial impact from water alone as the saturation fluid and less for the specific hydrocarbon saturants considered. Deionized water-saturated Indiana limestone samples were ~25% weaker than dry samples. Young's modulus was also reduced by ~25% with no significant change in Poisson's ratio. Samples that were saturated in deionized water for up to 8 weeks showed the same change in strength and Young's modulus as

samples that were saturated for less than 24 hours. A 9% potassium chloride solution weakened Salt Wash South samples and reduced Young's modulus by ~75% while increasing Poisson's ratio by ~25%. Berea Buff sandstone, when saturated with deionized water, showed ~20% reduction in strength with no substantial changes in Young's modulus and Poisson's ratio. Hypotheses for chemical interactions that occurred are provided, suggesting why aqueous compounds can substantially alter strength even in clay-poor rocks.

I would like to dedicate this work to my wife, April, for her endless sacrifices and support over the years; I am truly grateful.

TABLE OF CONTENTS

LIST OF TABLES

LIST OF SYMBOLS

Symbol	Meaning	Units
K_I	Stress intensity factor	$MN*m^{-3/2}$
σ_a	Remote applied stress	MN
Y	Constant that depends on loading geometry, crack configuration, etc.	--
α	Half of the crack length	m
K_{Ic}	Critical stress intensity	$MN*m^{-3/2}$
K_0	Initial stress intensity	$MN*m^{-3/2}$

ACKNOWLEDGMENTS

I would like to thank all people who have helped and inspired me throughout this project.

I am extremely thankful for my advisory committee (Dr. John McLennan, Dr. Sidney Green and Dr. Milind Deo) for their encouragement, guidance and insight throughout the research and writing process. Their help has enabled me to develop an understanding of the subject.

I would also like to thank the Schlumberger Center for Rock-Fluid Interaction in the Department of Chemical Engineering at the University of Utah for funding this project. This thesis would not have been possible without the diligent efforts of Dr. Green in obtaining continued funding from Schlumberger.

I am grateful for all of the people at TerraTek—A Schlumberger Company—whose patience and insight were invaluable during the experimental phase of this project. Particularly, I would like to thank Wes Martin, Jim Marquardt, Arnis Judzis and Dean Wilberg. I also appreciate the help of the many lab technicians who showed me how to prepare samples and conduct the experiments.

Lastly, I must acknowledge the love and support of my family; without them I could never have done this.

1 INTRODUCTION

1.1 Purpose

The effect of fluids on rock stiffness, strength, and fracture development is complicated and is still not well understood. Yet many applications involving rock-fluids interaction are of considerable interest, and often pose significant physical and economic impact on a given project. For instance, the instantaneous penetration rate during drilling, the formation of complex hydraulic fractures in highly heterogeneous formations, sand production that occurs with increasing water cut, as well as compaction and subsequent subsidence during water flooding in certain formations are of significant interest. For example, suppose that a formation is produced under primary recovery and then water flooding is started. If the water weakens the rock, compaction in the reservoir and subsidence at the surface may result. There is substantial literature showing the effect of aqueous fluids contacting certain clays, and more limited and scattered literature showing the effect of fluids on the strength of various rocks. In a few cases, mechanisms of strength gain or loss have considered capillary effects, pore pressure build-up or reduction, and thermal expansion/contraction. Mechanisms of strengthening/weakening and stiffening/ softening of rock, associated with contact with various solvents or additives have received less attention.

Given the complexity of the rocks considered and the wide range of physical and chemical phenomena that could be in play, the intent is to rationalize which mechanisms are most likely to be important (or at least under what conditions a particular mechanism may be dominant). This has been done by generating experimental data. Testing methodologies are discussed below.

1.2 Previous Work

Colback and Wiid (1965) conducted uniaxial and triaxial compression tests on quartzitic shale and quartzitic sandstone submerged in various fluids (a description of uniaxial and triaxial testing methods is given in section 1.3.1). Those measurements indicated that the compressive strengths of both of these rock suites were reduced by half when they were saturated with water. They postulated that, because the surface free-energy of a solid submerged in a liquid is a function of the surface tension of the liquid and given that the uniaxial compressive strength is a function of the uniaxial tensile strength which is a function of molecular cohesive strength, the role of the of the immersion fluid is to reduce the surface-free energy of the rock and hence its strength. In short, the reduction in strength from a dry to water-saturated condition of predominantly quartzitic rocks is governed by the reduction in surface free-energy of the quartz due to the presence of the liquid.

Atkinson (1979) considered stress corrosion cracking, subcritical crack growth that occurs in the presence of a chemically active environment, as the predominant process in strength reduction of single quartz crystals that were saturated with various fluids. Crack velocities within single quartz crystals were

carefully measured while water was introduced at the fracture tip. Experiments were conducted at temperatures ranging from 20°C to 80°C. Since crack tip stresses that cause crack growth are proportional to the stress intensity factor, a diagram was created that showed the change in crack velocity versus the stress intensity factor (Figure 1). The stress intensity factor is calculated by

$$K_I = \sigma_a Y \sqrt{\alpha} \quad (1)$$

where K_I is stress intensity factor, σ_a is the remote applied stress, Y is constant that depends on loading geometry, crack configuration, etc., and α is half of the crack length.

Atkinson's (1979) stress intensity factor-crack velocity diagram is split into three regions:

Region 1) This region is controlled by chemical reaction and the crack velocity increases rapidly.

Region 2) This region is controlled by the rate of diffusion of the reacting species to the fracture tip and the crack velocity is relatively constant.

Region 3) This region is controlled by a combination of the corrosive chemical environment and mechanical failure and the crack velocity increases very rapidly until crack propagation occurs.

These diagrams are considered significant in studying subcritical crack growth because they can be used to predict time-dependant failure properties and in the analysis of slow crack growth mechanisms (Wiederhorn 1978).

Atkinson and Meredith (1981) later studied the effects of the chemical environment on region 1 of Atkinson's stress intensity factor-crack velocity diagram (Figure 2). These authors found that the pH of the fluid present in the fracture altered the crack velocity. Specifically, they found that for quartz, crack extension initiated at low stress intensity when the sample was exposed to a high pH fluid and that as the pH decreased the stress intensity required to initiate crack velocity increased. In other words, crack growth at a finite velocity started at lower stress intensities in alkaline environments and at higher stress intensities as the environment becomes more acidic. Ultimately, they proposed the following weakening mechanism:

$$[H-O-H]+[-Si-O-Si-]=[-Si-OH.HO-Si-] \qquad (2)$$

The authors' conclusion was that hydrolysis of strongly bonded, highly stressed siloxane groups (-Si-O-Si-) occurs to form weakly joined, hydrogen-bonded, silanol groups (-Si-OH-). These silanol groups dissociate more readily then the siloxane groups that were previously in place. This weakening of strained bonds at a crack tip via a chemical reaction with the environment allows crack growth to occur at lower stresses. It was later found (Atkinson and Meredith 1984) that, in a water-saturated quartz crystal with a machined fracture, temperature also affected crack velocity in Region I of the Atkinson stress intensity factor-crack velocity diagram. When the temperature of the water was increased from 20°C to 200°C, at constant stress intensity, the crack velocity in the quartz samples increased by as much as 5 orders of magnitude. This increase in crack velocity

at increased temperatures can be explained by the lower activation enthalpy required for crack propagation.

Hawkins and McConnell (1992) conducted unconfined compression tests on 35 sandstones from various locations in Great Britain. They performed experiments on samples with varying saturation levels; ranging from dry to fully-saturated and were able to increase the moisture content (i.e., the amount of fluid in the pore space) in the rock samples by as little as 1%. The experiments showed that effects of saturation on strength and deformation varied greatly between the different clastic materials. They showed that weaker sandstones are not more sensitive to moisture content then strong sandstones. Alternatively, it was found that the degree of sensitivity to moisture content in their materials was controlled by the proportions of quartz and clay minerals that are present. They concluded that the rock microfabric only made a small contribution to strength alteration. The experiments also showed a marked difference in strength and deformation when a sandstone has as little as 1% moisture content.

Research has also been done on the effects of cementation on mechanical properties of dry sandstones from the Jauf and Unayzah formations in Saudi Arabia (Al-Tahini et al. 2006). These authors wanted to focus on the material that held the grains together. They compared strengths relative to this binding (cementing) material. Their research indicated that the change in mechanical properties was highly variable and dependent on the composition of and quantity of cementitious material. Not surprisingly, it was discovered that pure quartz overgrowths (silica that precipitates and forms within the grain

structure) in the samples played an important role in increasing the strength of a sample.

Vutukuri (1974) investigated the effects of fluid saturation on limestone. It was discovered that fluids significantly reduced the strength of the limestone evaluated. Vutukuri's hypothesis was similar to the observations of ColBack and Wiid; that the fluid caused a reduction in surface free energy causing a decrease in strength. He also suggested that liquids may dissolve material away from contact points, thus increasing the stress at those points, which aids crack propagation or development/initiation.

Stipp (1999) showed that calcite surfaces adsorb water and generate hydrolysis species that are chemisorbed to dangling bonds that are produced by cleavage (Figure 3). Similar to the aforementioned mechanism proposed by Atkinson and Meredith, tension is released from strained bonds allowing fracture propagation to more easily occur.

Clementz (1977) looked into the effects of water contacting clays present in-situ and at ways to stabilize these clays. He found that clay-rich formations were stabilized by adsorption of petroleum heavy ends. This "oil-wetting" caused the clay surfaces to become hydrophobic and proved to resist removal from common solvents such as brines and dilute HCl.

1.3 Methodology

1.3.1 Testing

Unconfined and triaxial compression tests were performed in accordance with ASTM D7012-10 or The Complete ISRM Suggested Methods for Rock Characterization, Testing and Monitoring, (2007). Samples were prepared with flat and parallel end surfaces with a length-to-diameter ratio of approximately 2. Any fluids that were present in the samples at the time of testing were allowed to move freely within the sample or allowed to drain from the sample. This testing method is commonly referred to as “drained conditions” and does not allow for pore pressure within the sample to change.

1.3.1.1 Unconfined Compressive Strength Test

Unconfined compressive strength (UCS) testing is one of the most basic testing methods for measuring the mechanical properties of rocks. Mechanical properties determined from this type of test include the unconfined compressive strength, Young’s modulus and Poisson’s ratio.

These UCS measurements were made using a servo-controlled piston that applies a load at a specified rate to the rock sample in the axial direction as seen in Figure 4. No radial pressure is applied to the sample in this type of test.

Axial and orthogonal radial deformations were measured and strains were determined. Stress is also determined from the applied axial force. The strength was determined from the axial stress at peak load (Figure 5). Young’s modulus

and Poisson's ratio are calculated from the stress-strain data. Test data were collected in real time at approximately 10 Hz.

1.3.1.2 Triaxial Compression Testing

Triaxial compression (TXC) is another common testing protocol used in civil, mining and petroleum industries and is used to assess in-situ rock performance characteristics. Young's modulus, Poisson's ratio and strength (as a function of hydrostatic confining pressure) were determined from a limited series of triaxial compression tests.

A TXC test is conducted in the same manner as an UCS test with the exception that a confining pressure is added to the sample, as seen in Figure 6. Force, displacement and pressure data are also recorded and analyzed in a similar fashion to the UCS test.

1.3.2 Deformation Mechanisms

As stress is applied during unconfined or triaxial compression testing, axial and radial deformations occur. Similarly, during the life of a hydrocarbon reservoir, changes in stress result from changes in formation fluid pressure, with attendant deformation. Rutter and Elliot (1976) provided a simple characterization of deformation mechanisms in rocks based on three general failure classes:

1) Cataclasis: processes involving fracturing and frictional sliding between rock grains or agglomerations of grains by application of pressure.

2) Dislocation mechanisms: at high stresses (relative to the shear modulus), creep is controlled by the movement of dislocations within the crystal lattice of the rock grains. Hence, dislocation mechanisms have a strong dependence on stress. High temperatures also strongly increase dislocation occurrence.
3) Diffusion-controlled creep processes: at relatively low stresses and high temperatures, creep occurs due to diffusion of atoms through the rock grains crystal lattice. This diffusion occurs at low temperatures (relative to the melting point) through the grain boundary (Cobble creep). As the temperature increases diffusion occurs throughout the grain (Nabarro-Herring creep).

Dislocation mechanisms and diffusion-controlled creep processes occur on relatively long time-scales and preferentially at high temperatures.

The relative importance of these processes at different conditions can be illustrated using deformation mechanism maps. Such maps have been published using a variety of different axes chosen from among, for example; grain size, temperature, stress and strain rate (Mohamed and Langdon 1974; Ashby 1972). Figures 7 and 8 show deformation maps developed based on temperature and stress for both calcite and quartz.

As can be seen in Figures 7 and 8, quartz and calcite deform differently at varying temperatures and pressures. It should be noted that they enter different phases of deformation at different pressure/temperatures but that the regions in which the deformation mechanisms exist are substantially different. For

instance, the dislocation creep region is much smaller in calcite than in quartz, but quartz does not have a cobble creep mechanism at all.

Of the three previously mentioned deformation mechanisms, none explicitly incorporate the effects of fluid on the deformation process. The following fluid-related deformation mechanisms are commonly considered:

1) Fluid-Modified Crystal Plasticity: Solid phase diffusion, such as Cobble creep and Nabarro-Herring creep are slow processes and occurs preferentially at high homologue temperatures (temperatures relative to the melting point of the material.) Water inclusions in the crystal lattice will facilitate diffusion. Ingress of fluid (ions) into the crystal lattice is possible but diffusion rates are slow. The solid material is not removed from by the fluid but instead diffuses to another location in the direction of the stress.
2) Pressure Solution: Pressure solution requires diffusion of dissolved species away from a highly stress zone, through permeable channels such as fractures or interconnected pores (Figure 9). Pressure solution occurs because diffusive mass transport is aided by the presence of a fluid at the grain boundaries. Since time-scales for diffusion scale as the inverse third power of the relevant length scale (e.g., grain size) so pressure solution would be favored in fine-grained structures rather than coarse-grained structures. Pressure solution is a mechanism that is predominant in the earth's crust (Rutter 1983) but is unlikely to be the dominant mechanism in rapid processes associated with many rock engineering activities.

3) Chemical Dissolution: This entails production of new substances by chemical reactions. One example would be hydrochloric acid and limestone reacting to form water, CO_2 gas and aqueous calcium chloride. This reaction occurs quickly and continues until the acid is spent. This reaction is commonly used in the petroleum industry to create wormholes or etched fracture surfaces to increase hydrocarbon productivity in carbonates. For systems that do not react readily, the volume of rock removed is small and unlikely to lead to the magnitude of change over a short time period. In this case, the phenomena will be diffusion rate limited and thus requires relatively long time scales.
4) Stress Corrosion Cracking: Subcritical crack growth is the extension of one or more pre-existing fracture(s) of material at stress levels below the critical stress intensity factor. Failure under constant load, below the nominal critical stress, results, for example, from specific environmental conditions such as aggressive chemical action or elevated temperatures. Here, we are specifically concerned with situations where the crack velocity is controlled by chemical interactions at or around the crack tip and this is referred to as stress corrosion cracking.
5) Lubrication: Granular flow is the movement of grains, by translation or rotation, to allow deformation. Fluids may aid this process by reducing the friction between the grains through lubrication. Lubrication definitely aids in deformation after failure has occurred and the grains are moving. Its

role before dynamic friction is in place is certain but the degree of contribution is not quantified in this research.

6) Capillary Action: Capillary forces result because there is a net attractive force between grains due to saturation wetting phase with two immiscible fluids, as illustrated in Figure 10. This force is greatest at low saturations and declines as saturation increases. Any chemical modification leading to reduced capillary pressure (reduction in interfacial tension or wetting angle) will lead to reduced strength compared to a partially saturated system. Capillary forces will not exist in situations of 100% saturation by a single fluid, or 100% saturation of fully miscible fluids.

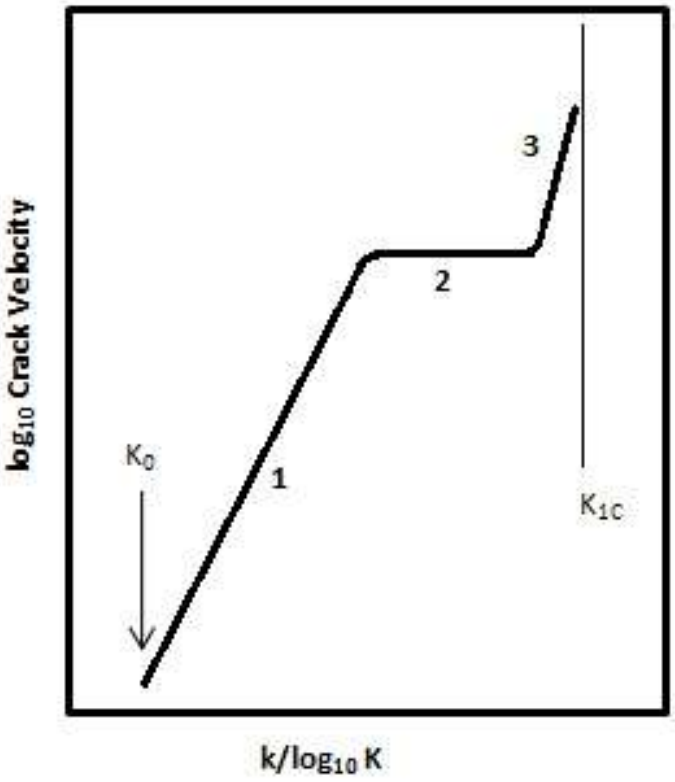

Figure 1 Stress intensity factor-crack velocity diagram representing tensile fracture of glasses and ceramics in a chemically reactive environment. Region 1 is controlled by the reaction rate between the surface and the reactive environment. Region 2 is controlled by the diffusion rate of the chemical species to the fracture tip. Region 3 is controlled by a mixture of the corrosive environment and mechanical failure. K_0 is the initial stress intensity. K_{1C} is critical stress intensity. (Modified from Atkinson 1979)

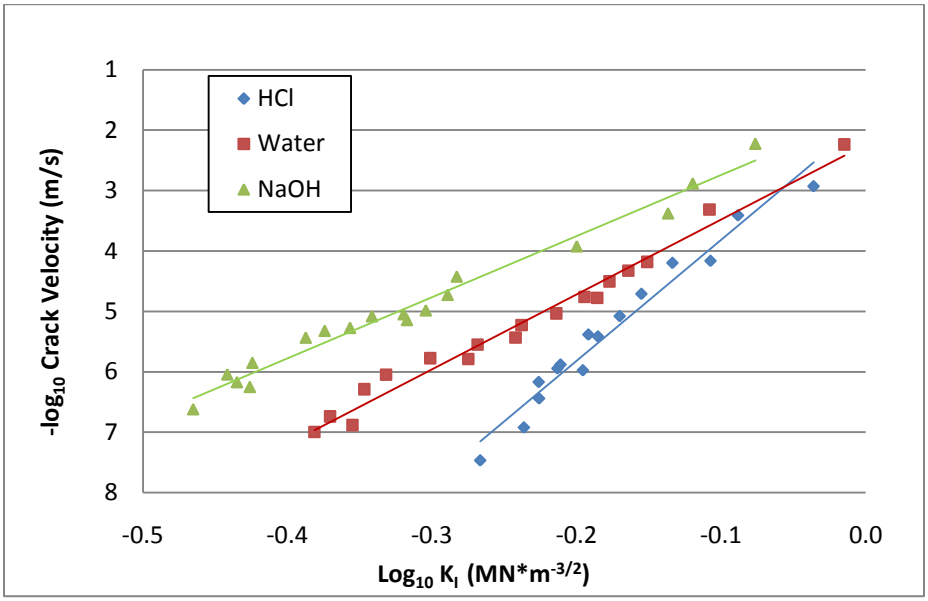

Figure 2 Data representing the change in crack velocity in quartz due to pH in the phase I region of the stress intensity factor-crack velocity diagram. Solid lines represent a least squared fit to the data. (Modified after Atkinson and Meredith 1981)

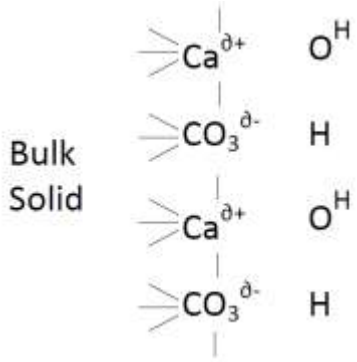

Figure 3 Illustration of hydrolysis species that are chemisorbed to dangling bonds in calcite. The water molecules align themselves along the calcite molecules and chemisorbs onto the surface. These newly created bonds relieve tension from the strained bonds which allows for fracture propagation to more easily occur. (Modified from Stipp 1999)

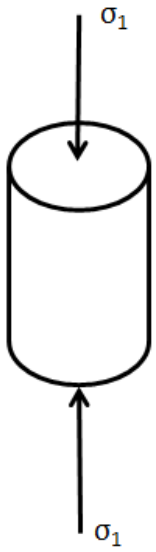

Figure 4 Unconfined compressive strength test. Stress is applied to a rock sample axially (σ_1) without any radial stress being applied to the rock sample.

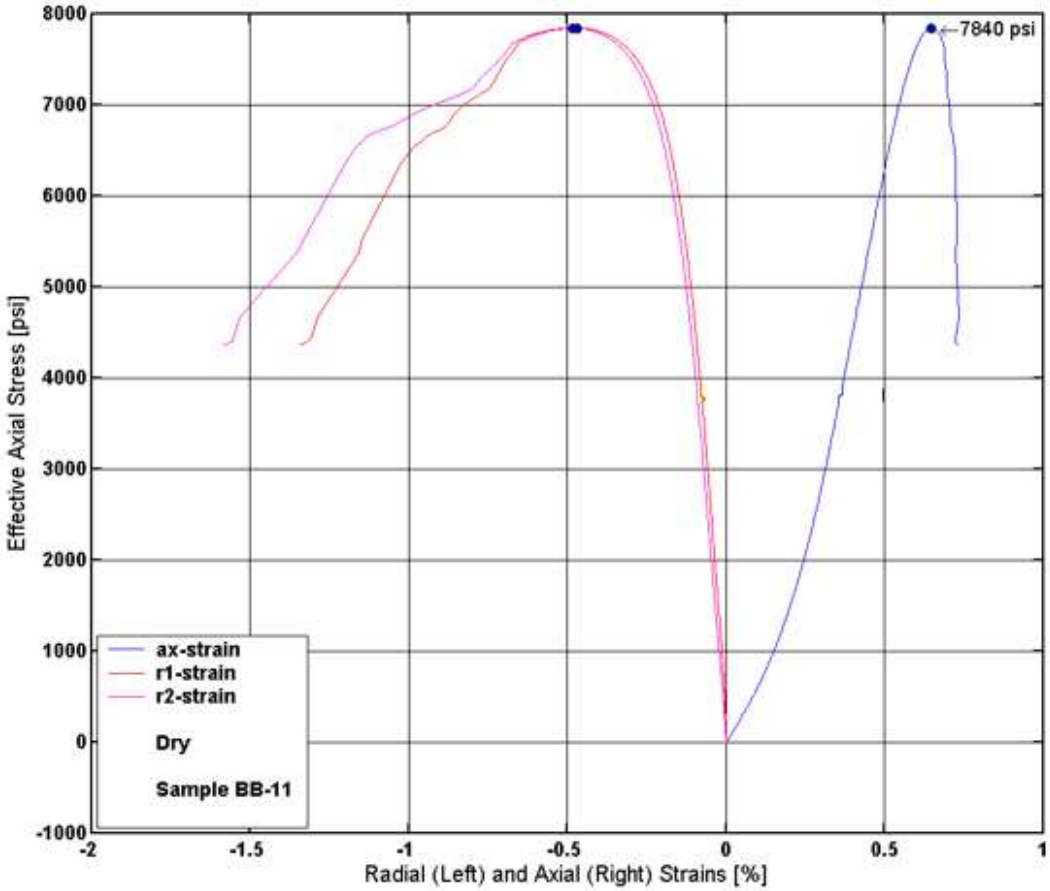

Figure 5 Stress-strain curves for a sample of Berea Buff obtained during a UCS test. The two lines on the left (pink and orange) represent the radial strain on the sample during testing. The line on the right (blue) represents the axial strain on the sample during testing. This sample failed at 7840 psi, as indicated on the graph.

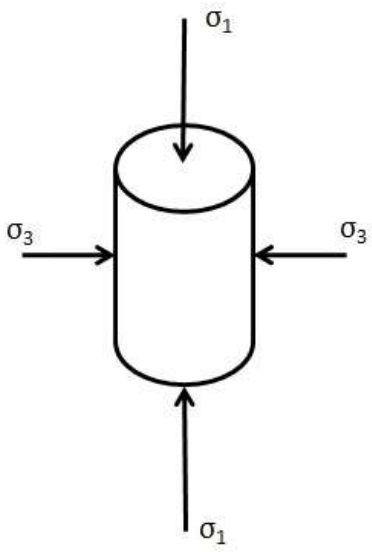

Figure 6 Triaxial compression testing. Stress is applied to a rock sample axially (σ_1) with a confining pressure (σ_3).

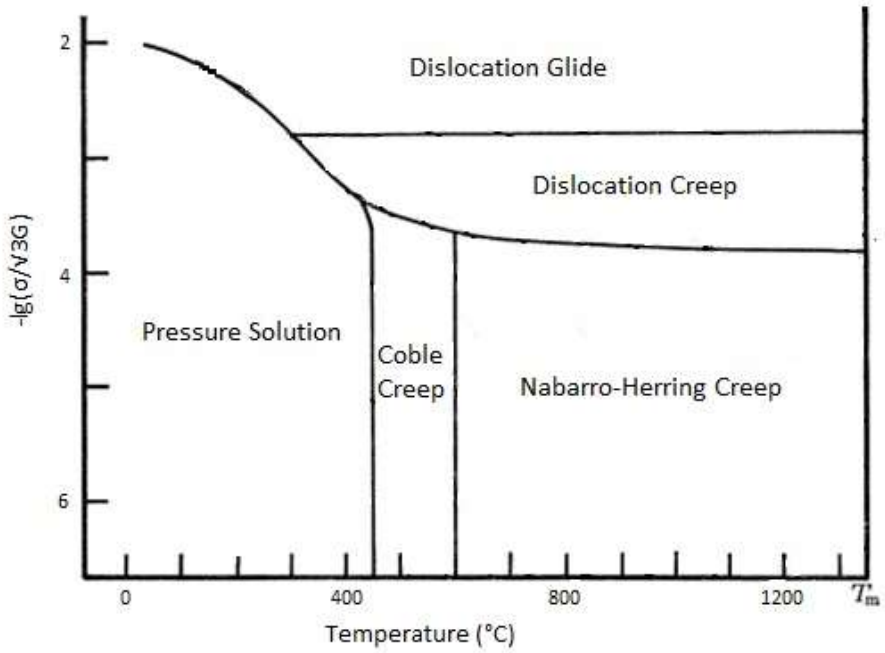

Figure 7 Deformation mechanism map based on temperature and stress for Calcite. Each region of the map identifies the dominant deformation mechanism under the specified conditions. (Modified from Rutter 1976)

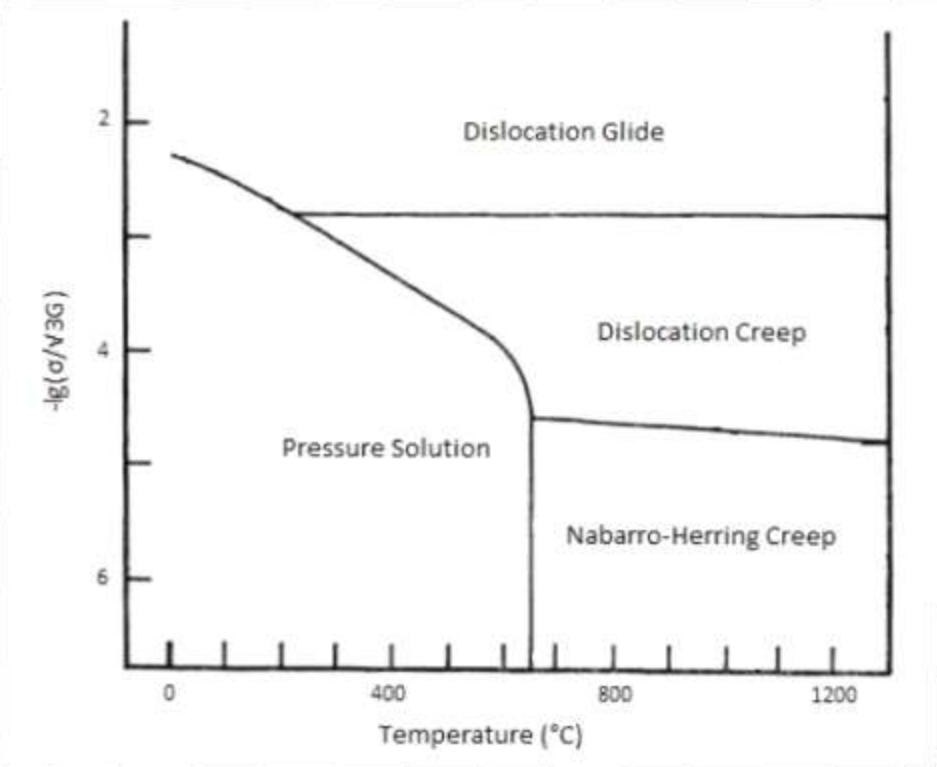

Figure 8 Deformation mechanism map based on temperature and stress for quartz. Each region of the map identifies the dominant deformation mechanism under the specified conditions. (Modified from Rutter 1976)

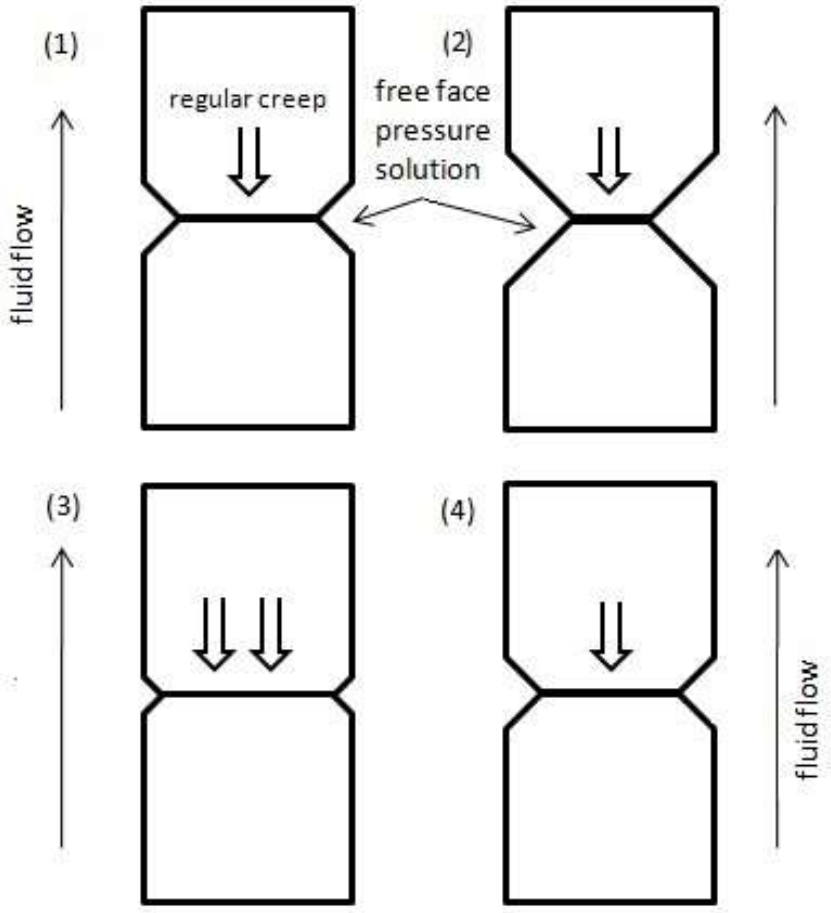

Figure 9 Illustration of the pressure dissolution mechanism. (1) Dissolution occurs in pore spaces away from contact point. (2) The support "neck" continues to thin due to dissolution. (3) As the "neck" continues to thin a critical stress is reached causing a small and rapid brittle compaction. (4) The process starts over again. (Modified from Le Guen et al. 2007)

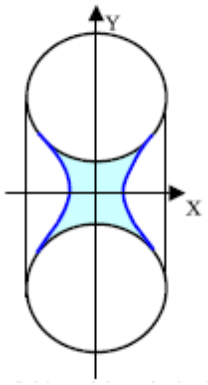

Figure 10 Illustration of capillary forces acting on water and two idealized rock grains.

2 EXPERIMENTAL PROGRAM

2.1 Sample Selection

Three rock types were chosen for this project: Indiana limestone, Salt Wash South sandstone and Berea Buff sandstone. Indiana limestone was chosen since it is touted as a homogeneous type of limestone that is fairly well understood and is analogous to many other types of limestone. Salt Wash South sandstone is a very weak, clay-cemented, fine-grained sandstone. It might be considered to be analogous to some Gulf of Mexico sandstones. Berea Buff sandstone was chosen because it is a locally homogeneous, relatively strong clastic sandstone.

2.2 Sample Preparation

All of the samples were received as large-diameter cores approximately 10 inches in diameter and of varying length. Smaller plugs were cut from these cores. These plugs were cored to produce cylinders with a nominal diameter of 1 inch. They were then cut and end ground flat and parallel to a nominal length of 2 inches. Samples were cored in groups from the same lithologic layer in the large diameter cores to maintain some degree of similarity. Each sample was then CT-scanned to ensure relative homogeneity within the sample (Appendix A).

Each sample was oven-dried at 60°C. Sample weight was measured daily until it was constant within a prescribed tolerance of 0.01 grams for at least three

consecutive days; implying that the sample was essentially dry. In reality, there was some residual water that is held in clays, capillaries, etc. The samples were then stored in a desiccator. After drying, the porosity of each sample was measured using helium and standard Boyle's law techniques. The permeability of each sample to nitrogen was measured.

Bulk rock and clay mineralogy were determined using X-Ray diffraction (XRD). It was assumed that the mineralogy of the selected samples was representative of the mineralogy of the entire sample set. This assumption is reasonable because each sample group came from the same piece of core. However, the variable nature of any rock is acknowledged.

Some samples were tested dry. Others were saturated with deionized water, a potassium chloride (KCl) solution or odorless mineral spirits. Where appropriate, samples were vacuum-saturated. Masses were measured before and after saturation as well as immediately before testing to asses if they were fully saturated—using rudimentary procedures. Most samples were tested within 24 hours of saturation.

2.3 Sample Description

In order to properly understand the chemical effects of fluids on the mechanical properties of rocks a sound understanding of the chemical composition, permeability and porosity of a rock is required.

2.3.1 X-Ray Diffraction

X-ray diffraction is a well understood and commonly used technique in the earth sciences for characterizing species within a rock specimen and for quantifying the percentage of that species in the sample.

2.3.1.1 Indiana Limestone

As can be seen in Table 1, Indiana limestone is primary composed of calcite ($CaCO_3$). Of particular interest is the low clay content. The clay-sized particles, illite and mica mixtures, will not swell in the presence of water.

2.3.1.2 Salt Wash South Sandstone

As is typical with all sandstones, Salt Wash South is primarily composed of quartz (SiO_2). Table 2 shows that Salt Wash South contains 8% clays and it should be noted that the clay content is composed of smectite and illite/smectite. Both of these clays are known to be very sensitive to water and cause weakening within a rock sample via clay swelling.

2.3.1.3 Berea Buff Sandstone

Similar to the Salt Wash South sandstone, Berea Buff sandstone is primarily composed of quartz with almost identical amounts of K-feldspar and plagioclase. The Berea Buff has less clay thean the Salt Wash South and the clays that are present do not substantially swell when exposed to water.

2.3.2 Permeability and Porosity

Permeability and porosity measurements were taken on each sample before testing as mentioned above and can be seen in Appendix B. Table 4 reports the average porosity and gas permeability.

2.3.3 Thin Sections

Rock samples were initially impregnated with a low-viscosity fluorescent red-dye epoxy resin under high vacuum to highlight porosity types. The impregnated samples were surfaced, mounted to standard (24 mm by 46 mm) thin section slides, and ground to a thickness of approximately 30 microns. The thin sections were then stained with a mixture of potassium ferricyanide and Alizarin Red “S” to aid in identification of carbonate minerals.

2.3.3.1 Indiana Limestone

Figures 11 and 12 show various rounded calcareous fossil fragments (echinoderm, brachiopod, bryozoan) with dark algal-micrite coatings. The oolitic limestone is strongly cemented by sparry calcite crystals (the clear crystals). There is some interparticle porosity (highlighted by the magenta-dyed epoxy).

2.3.3.2 Salt Wash South Sandstone

Figures 13 and 14 are thin section images of Salt Wash South sandstone. Note the 1 mm scale in the lower right corner of Figure 13. A greater magnification view is shown in Figure 14. In these thin section images ‘Q‘ indicates quartz and ‘srf’ indicates a rock fragment. Porosity is shown in magenta. Of note are the maturity of the grains (well rounded) and the high

porosity with little grain contact. The clays that are present are fluid sensitive and this material will disaggregate completely and instantly in water. The circles show some restricted grain contacts that may be partially infilled with siliceous cement. The arrows indicate the cracks prone to failure.

2.3.3.3 Berea Buff Sandstone

Figures 15 and 16 are thin section images of Berea Buff sandstone. Again, porosity is shown in magenta. Convex-concave (cc) grain contacts are seen as well as some penetrating mineralized (pm) and penetrating tangential (pc) grain contacts. Some altered feldspars (F) are also seen as is a resistant Chert (Ch) fragment. The Berea Buff is a dirty sandstone (meaning it has a reasonably high clay content). The heavy minerals may contribute to its coloration. Unlike the Salt Wash South sandstone, the individual grains are quite angular to sub-angular, suggesting much greater frictional resistance to stress. The grain contacts are much more extensive than in the Salt Wash South.

Table 1 X-Ray diffraction results for Indiana limestone.

MINERALOGY	WEIGHT %
QUARTZ	3
CALCITE	94
TOTAL NON-CLAY	*98*
ILLITE+MICA	2
TOTAL CLAY	*2*

Table 2 X-Ray diffraction results for Salt Wash South.

MINERALOGY	WEIGHT %
QUARTZ	86
K-FELDSPAR	3
PLAGIOCLASE	3
TOTAL NON-CLAY	*92*
SMECTITE	1
ILLITE/SMECTITE (I/S)	2
ILLITE+MICA	4
KAOLINITE	1
TOTAL CLAY	*8*

Table 3 X-Ray diffraction results for Berea Buff sandstone.

MINERALOGY	WEIGHT %
QUARTZ	90
K-FELDSPAR	3
PLAGIOCLASE	2
TOTAL NON-CLAY	*95*
ILLITE+MICA	2
KAOLINITE	2
CHLORITE	1
TOTAL CLAY	*5*

Table 4 Average permeability and porosity for Indiana Limestone, Salt Wash South Sandstone and Berea Buff Sandstone samples used for expermintation.

Rock Type	Porosity (%)	Standard Deviation	Gas Permeability (mD)	Standard Deviation
Indiana Limestone	16.0	1.1	6.2	1.90
Salt Wash South Sandstone	32.3	0.6	2399	197
Berea Buff Sandstone	21.9	0.9	381	135

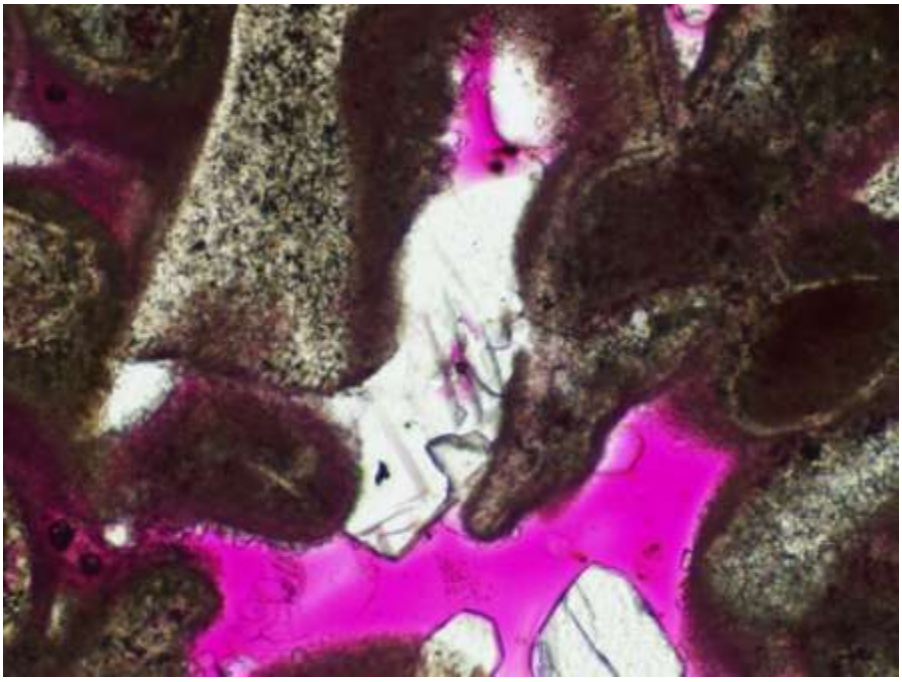

Figure 11 Thin section image of Indiana limestone. This is taken at 5x magnification with a view diameter of 1.72 mm.

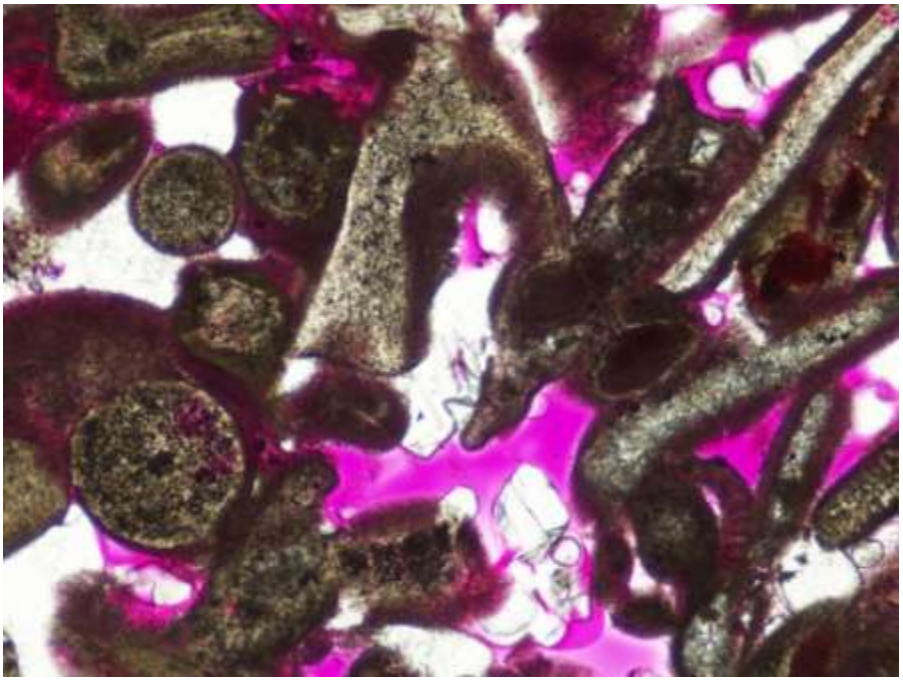

Figure 12 Thin section image of Indiana limestone. This is taken at 2.5x magnification with a view diameter of 3.44 mm.

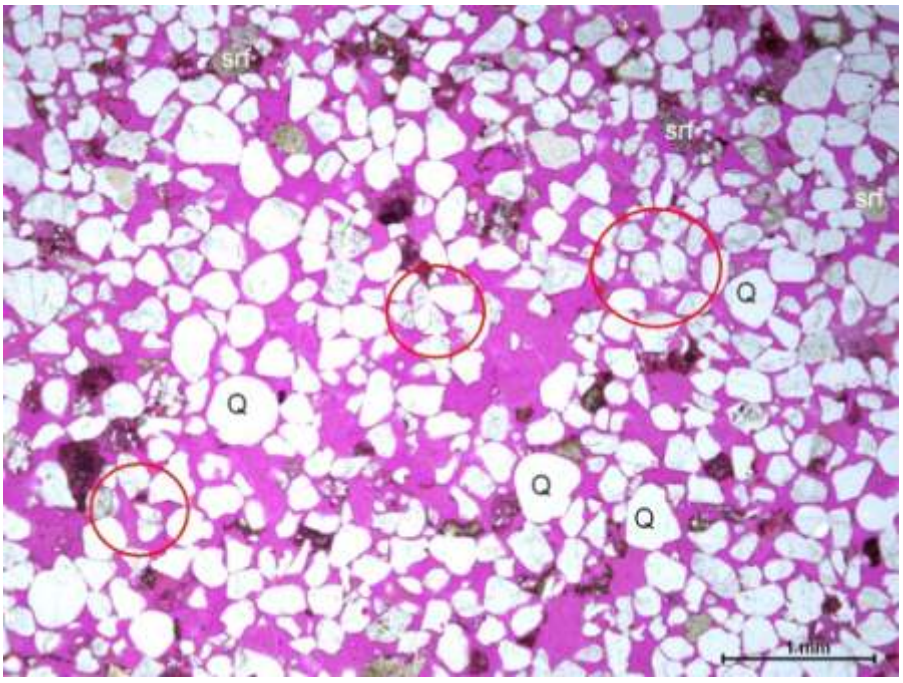

Figure 13 Thin section image of Salt Wash South.

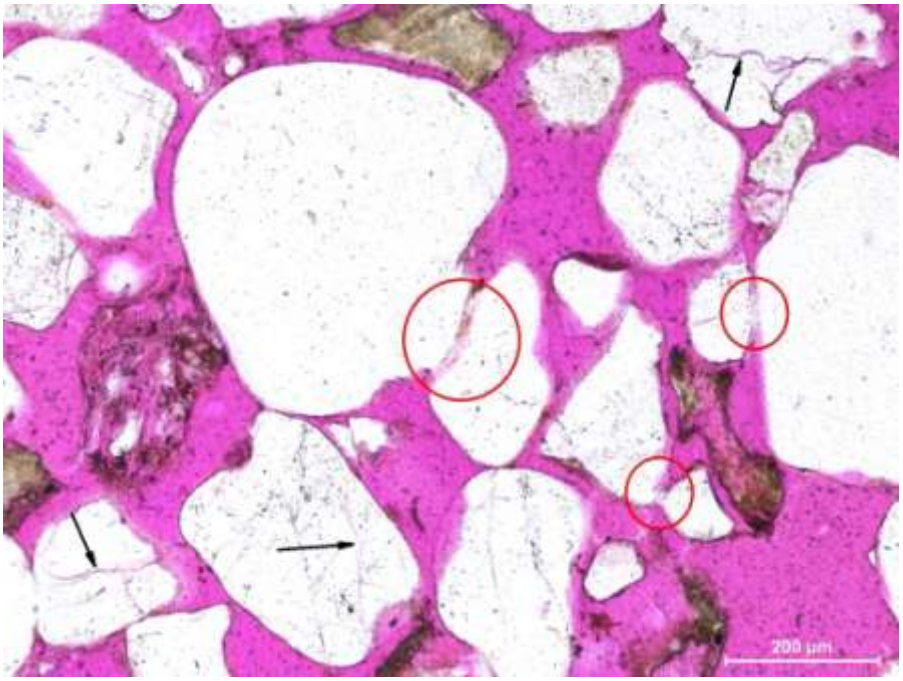

Figure 14 Thin section image of Salt Wash South Sandstone. This image is a magnification of Figure 13

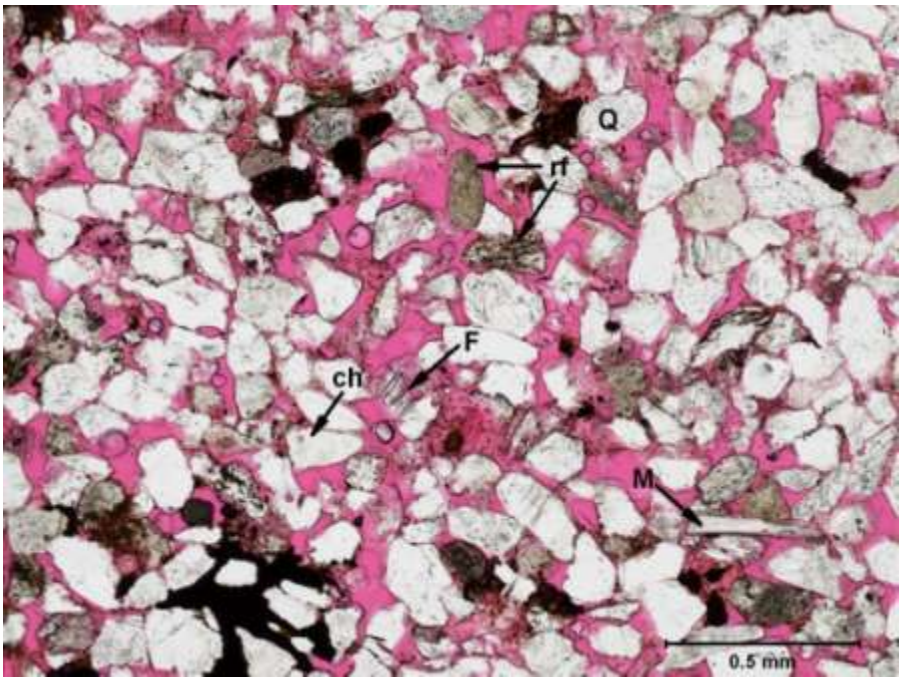

Figure 15 Thin section image of Berea Buff sandstone.

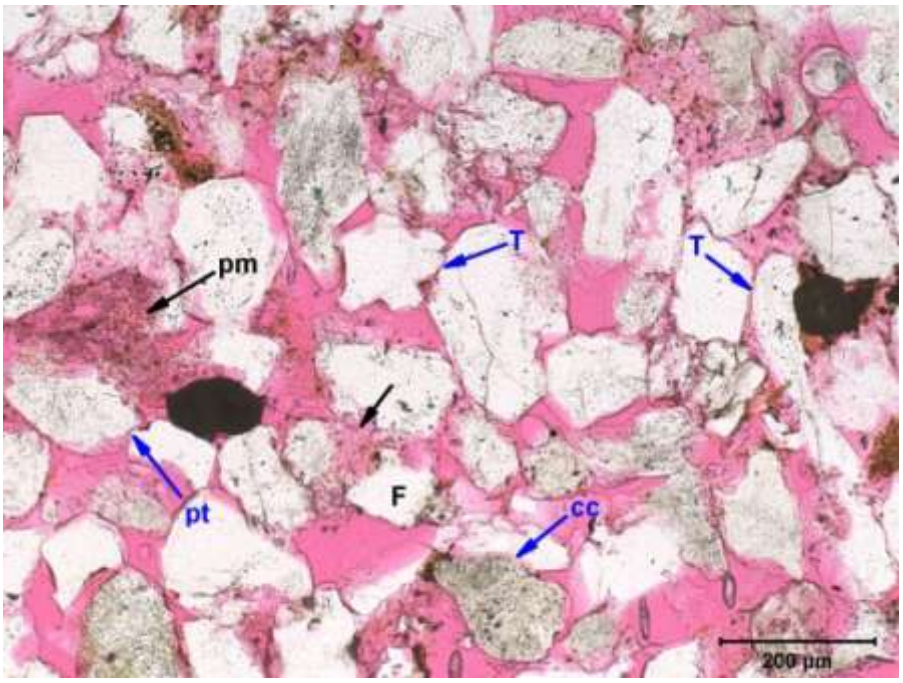

Figure 16 Thin section image of Berea Buff sandstone. This is a magnified view of Figure 15.

3 RESULTS

3.1 Indiana Limestone

Figures 17 through 19 show unconfined compressive strength data for Indiana limestone. As can be seen from Figure 17, OMS had no effect on the mechanical failure of the Indiana limestone (peak strength). The KCl solution and the deionized water produced statistically identical results and reduced the rock strength by roughly 22%. Young's modulus shows similar trends (Figure 18); OMS had no effect on the Young's modulus while the KCl solution and deionized water reduced the modulus by nearly 25%. There is no significant statistical change in Poisson's ratio with the varying saturation conditions (Figure 19).

It was next questioned whether there were any time-related considerations for strength alteration of rocks in the presence of fluids. UCS tests were conducted on samples saturated in deionized water for one, two and eight weeks. Although there are slight variances in the strength of the rocks, there does not seem to be any significant variance in the rocks that were saturated for one, two or eight weeks compared to the rocks that were saturated for less than 24 hours (Figure 20).

To recap, the results of the unconfined compressive testing indicate that, of the saturation fluids chosen, water (either deionized or with 3% KCl) substantially reduces strength and Young's modulus of Indiana limestone. The

testing also shows that there are no significant additional changes to the strength and stiffness of the limestone over longer time scales; thus, leading to the conclusion that the effect happens relatively quickly. This conclusion implies that pressure solution and fluid-modified crystal plasticity are unlikely to be the mechanisms that cause the alteration in strength and Young's modulus over the time periods considered. Although pressure solution is not considered viable in these experiments, it could be significant under realistic reservoir conditions (temperatures, pressures and time-scales).

Two Indiana limestone samples were also tested under triaxial loading conditions with a confining pressure of 14,000 psi. This pressure was chosen because previous measurements by others indicated that it would simulate pressure at great depths without causing pore compaction to occur. Peak strength for the Indiana limestone samples could not be obtained from the triaxial compression testing because the samples strain hardened. However, a closer evaluation of the axial stress versus volumetric strain curve (Figure 21) showed that samples that were saturated with deionized water behaved differently during the loading process when compared to the dry samples. This was expected because the dry sample has a higher bulk modulus. Although this finding is interesting, and probobly warrents further investigation, it was not further explored here.

3.2 Salt Wash South Sandstone

Unconfined compression testing was conducted on the Salt Wash South sandstone samples. This sandstone is known to completely disaggregate when

saturated with deionized water. Due to clay effects, previous experience established that this material will remain consolidated enough for testing provided that the aqueous saturant contained at least 9% KCl.

Figures 22 through 24 show the results for each saturant. The reduction of peak strength due to OMS saturation was approximately 8%. The 9% KCl solution produced a much larger reduction in peak strength at nearly 75% (Figure 22). Young's modulus for the Salt Wash South sandstone was reduced by both OMS and the 9% KCl solution by ~25% and ~75%, respectively (Figure 23). Interestingly, Poisson's ratio was unaffected by OMS saturation and increased by 25% when saturated in the 9% KCl solution (Figure 24). This probably is a reflection of clay sensitivity to the saturating fluid.

Of all the rocks that were chosen for testing, the Salt Wash South sandstone showed the most sensitivity to fluid saturation. This is not surprising considering that the XRD showed that Salt Wash South contains water sensitive clays.

3.3 Berea Buff Sandstone

Figures 25 through 27 show unconfined compressive strength data for Berea Buff samples. This testing showed that the OMS and deionized water reduced the unconfined compressive strength of the Berea Buff sandstone samples by nearly 10% and 20%, respectively (Figure 25). While there can be arguments as to the statistical veracity of this data, it is inferred that this is not strictly sample variability. Although the saturation fluids caused a reduction in the peak strength of the Berea samples, the fluids seem to have had no effect on

Young's modulus (Figure 26). As with the limestone samples, Poisson's ratio (Figure 27) was largely unaffected by the saturation fluids.

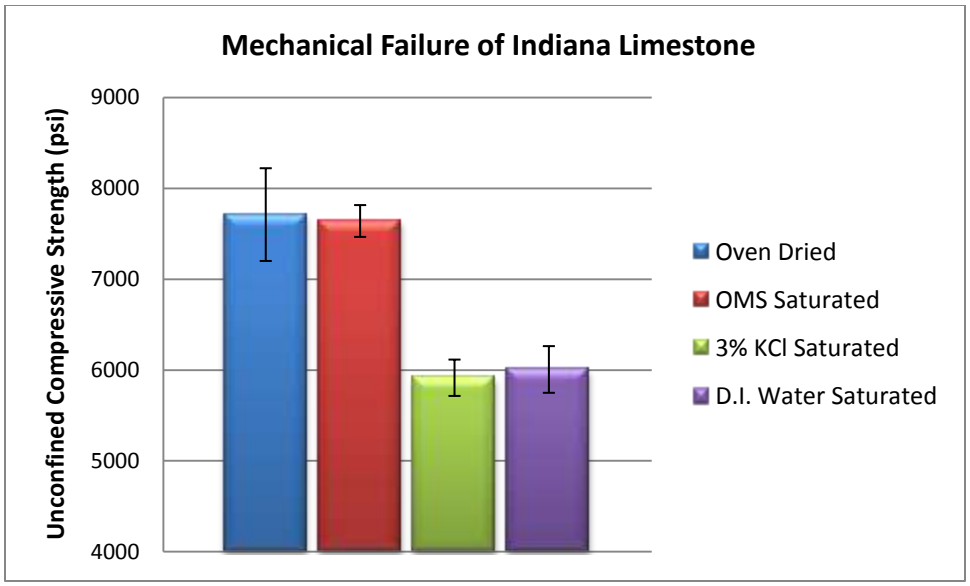

Figure 17 Mechanical failure of Indiana limestone samples obtained from UCS testing under various saturation conditions. Standard deviation values are also represented.

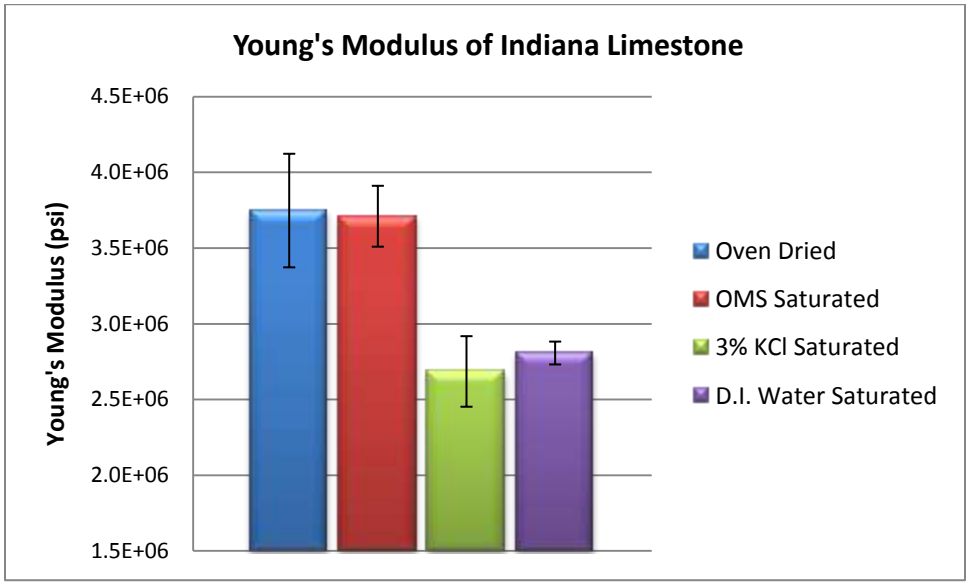

Figure 18 Young's modulus of Indiana limestone samples obtained from UCS testing under various saturation conditions. Standard deviation values are also represented.

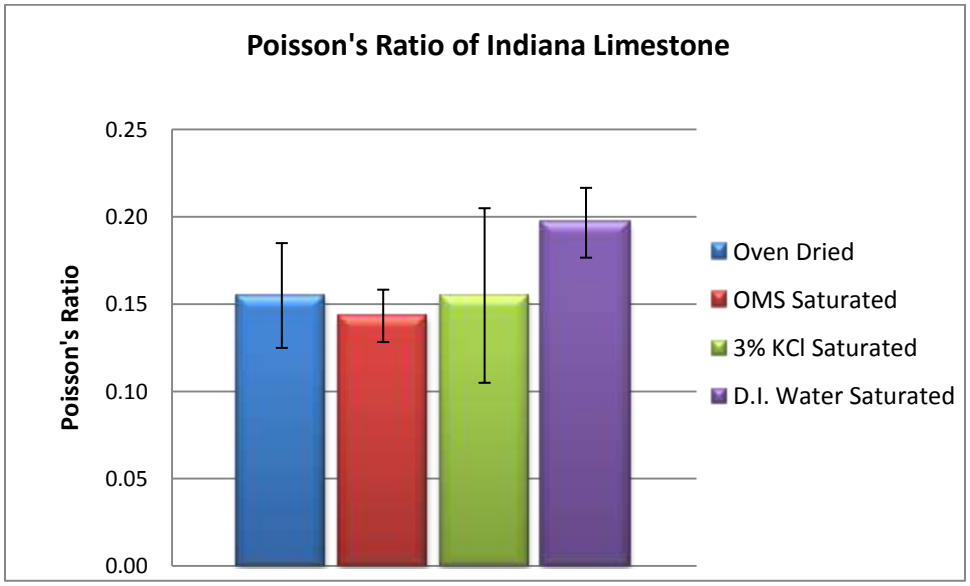

Figure 19 Poisson's ratio of Indiana limestone samples obtained from UCS testing under various saturation conditions. Standard deviation values are also represented.

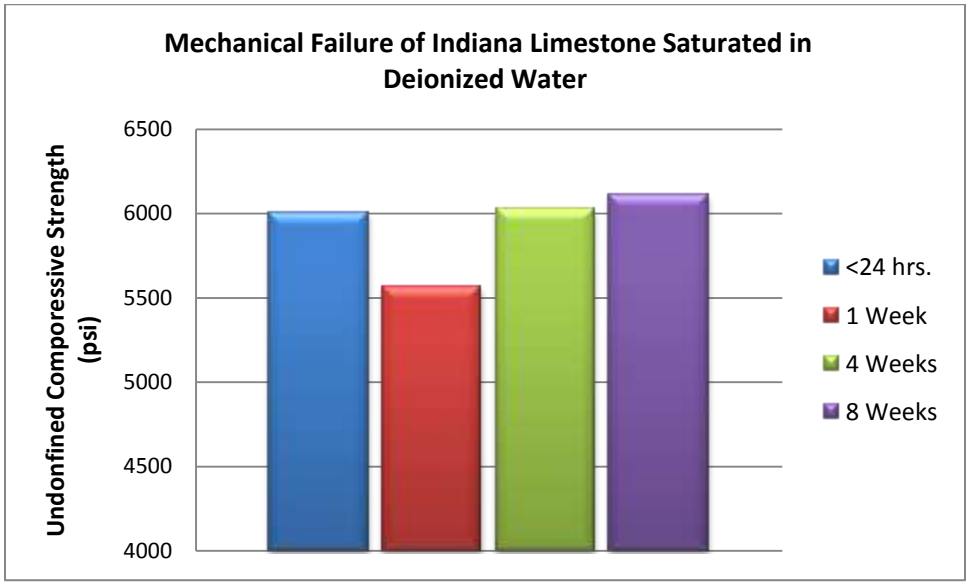

Figure 20 Peak strength of Indiana limestone samples obtained from UCS testing. Samples were saturated in deionized water for various lengths of time to determine if the change in strength is time dependent.

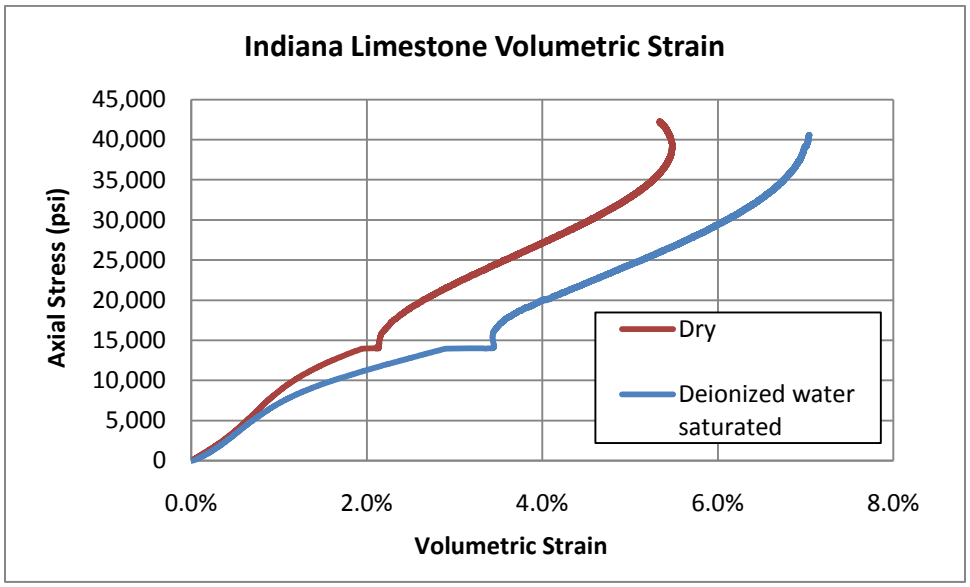

Figure 21 Axial stress versus volumetric strain obtained from TXC testing.

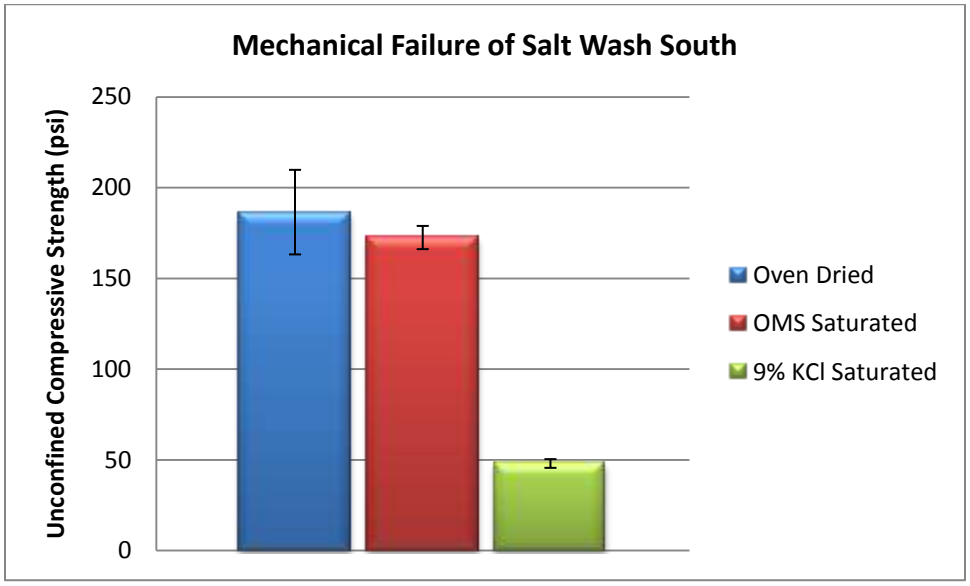

Figure 22 Mechanical failure of Salt Wash South sandstone samples obtained from unconfined compression testing under various saturation conditions. Standard deviation values are also represented.

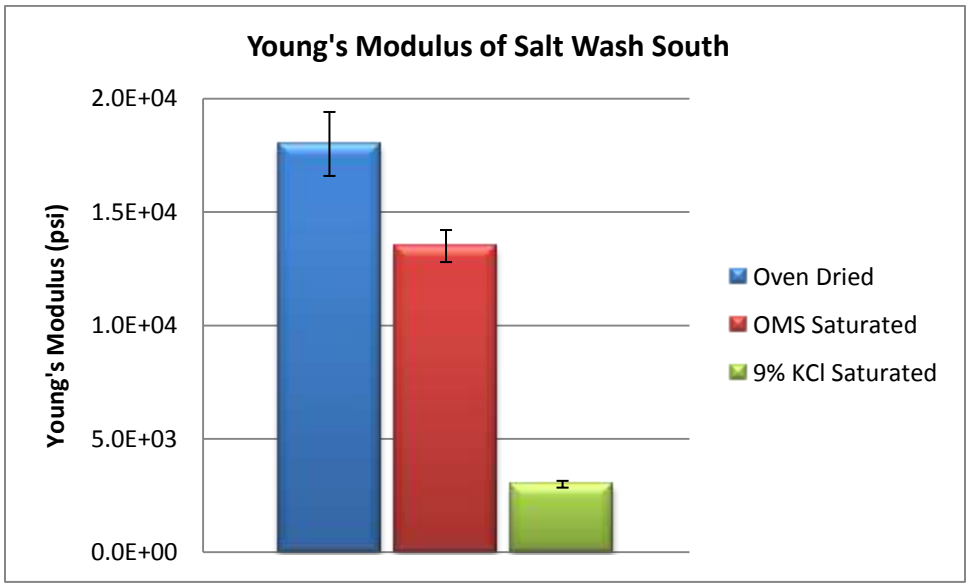

Figure 23 Young's modulus of Salt Wash South sandstone samples obtained from UCS testing under various saturation conditions. Standard deviation values are also represented.

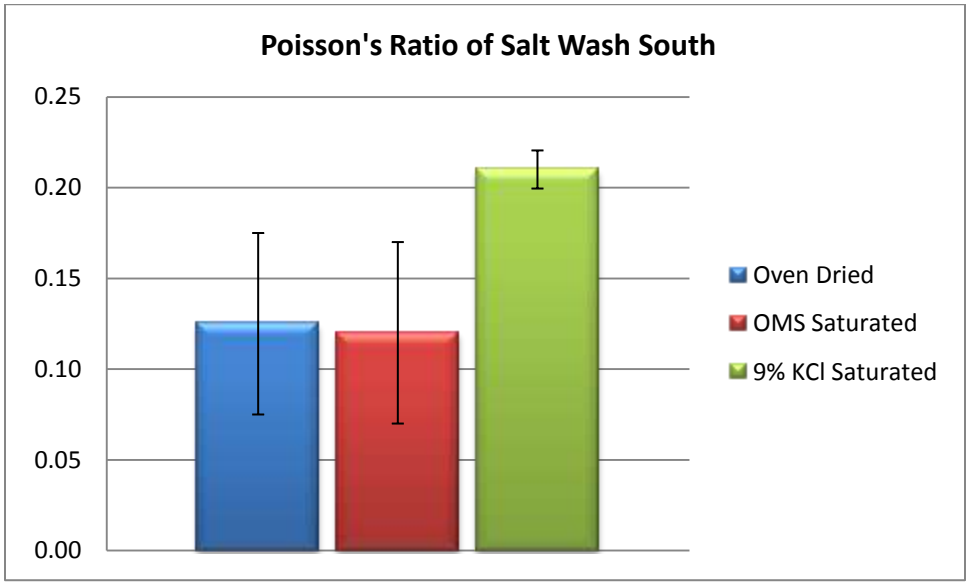

Figure 24 Poisson's ratio of Salt Wash South sandstone samples obtained from UCS testing under various saturation conditions. Standard deviation values are also represented.

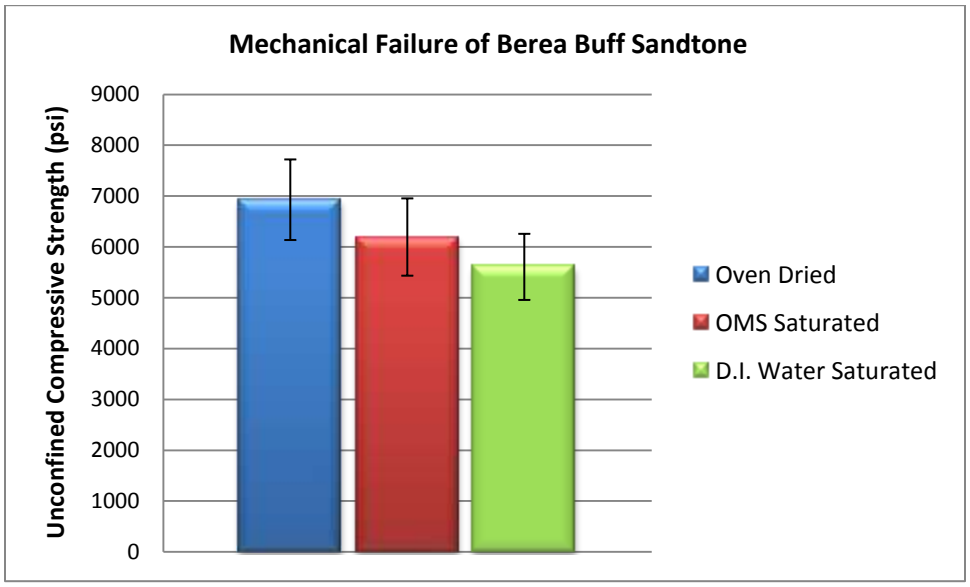

Figure 25 Peak Strength of Berea sandstone samples obtained from UCS testing under various saturation conditions. Standard deviation values are also represented.

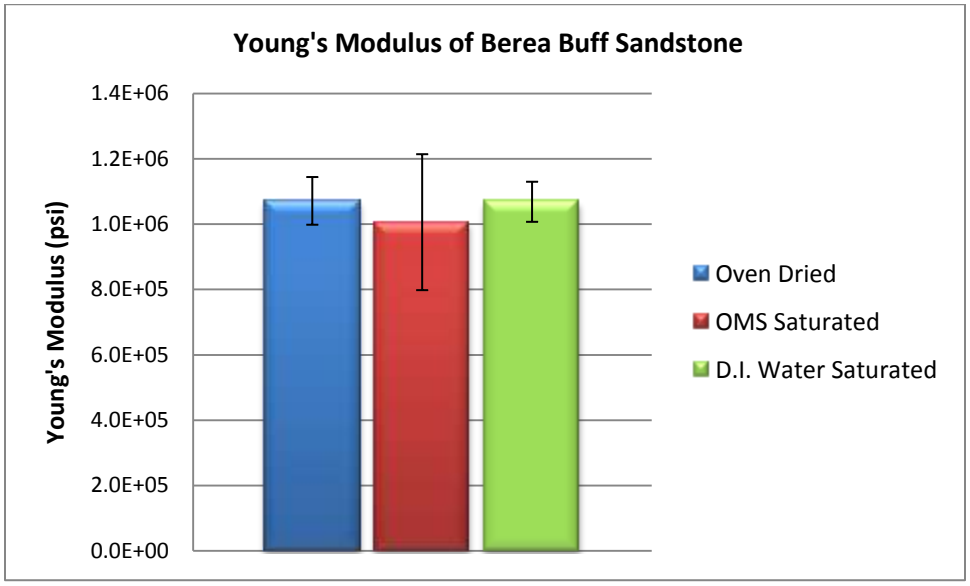

Figure 26 Young's modulus of Berea sandstone samples obtained from UCS testing under various saturation conditions. Standard deviation values are also represented.

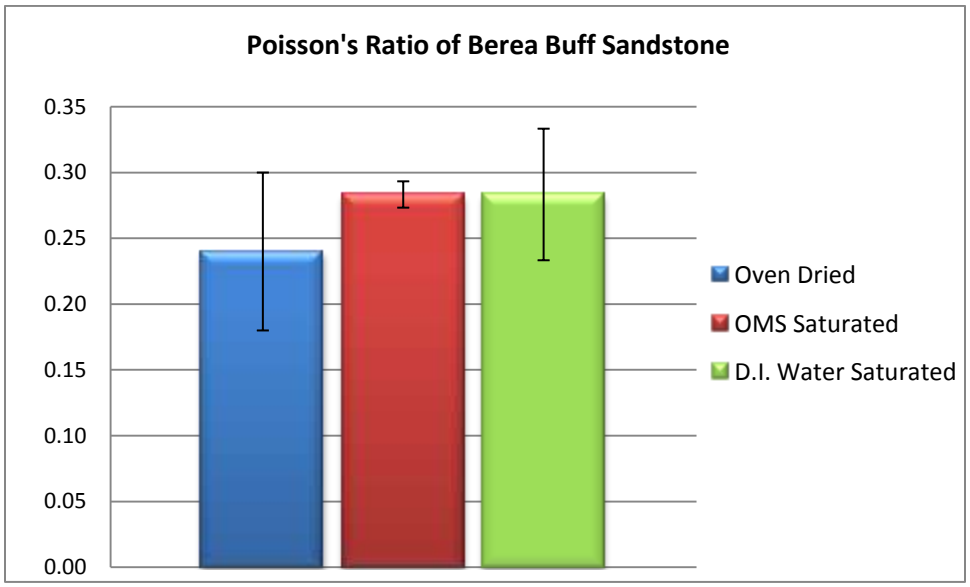

Figure 27 Poisson's ratio of Berea sandstone samples obtained from UCS testing under various saturation conditions. Standard deviation values are also represented.

4 DISCUSSION OF RESULTS

Of the six fluid-related deformation mechanisms mentioned previously, two are able to be discarded as a dominant weakening mechanism due to the short saturation and testing times: fluid-modified crystal plasticity and pressure solution. Chemical dissolution can also be disregarded in all cases because reaction rates are relatively slow between the rocks samples and fluids. The fluids used in the testing were known to have low solubility with the minerals in the rock samples. Capillary effects are also considered irrelevant because all of samples were dry or fully saturated. Observations of significant weakening using different fluids with similar viscosities (viscosities at room temperature: deionized water, 1.002 cP; OMS, 1.31 cP; KCl solutions were considered to have same viscosity as the deionized water) suggest that simple lubrication effects are not dominant. Therefore, it is suggested that simple mechanical lubrication between grains is not the dominant factor in differentiating short-term fluid-related strength degradation.

By elimination, subcritical crack growth caused by stress corrosion appears to be a dominant weakening mechanism for Indiana limestone. It appears that the chemisorbtion mechanism proposed by Stipp (1999) is responsible for the weakened limestone samples since the limestone samples that were saturated with water were weaker than any of the other samples. This

chemical mechanism seems reasonable when looking at the thin sections since the pore space (the area where the fluid would be present) is adjacent to the calcite crystals that are present and that are acting as a binding agent for the calcite grains.

Since the Salt Wash South samples are held together primarily by water sensitive clay, and the OMS had no effect on the sample, clay swelling is deemed reasonable as a weakening mechanism.

Similar to the Indiana limestone, stress corrosion appears to be the dominate deformation mechanism for the Berea Buff sandstone. The Berea Buff sandstone was weakened the most by the presence of water. This suggests that the silanol groups, that are formed when quartz is exposed to water, create a chemically active alkaline environment. (Atkinson and Meredith 1981) This reactive environment allows for crack velocity to increase and failure to occur at a lower stress/pressure level. Thin sections also support this hypothesis because the pore space is primarily adjacent to the quartz crystals, thus allowing the reaction to occur.

In all three rock types it is difficult to discern where the deformation is occurring; at the contact points between crystals/clays and grains or within the grains themselves.

5 CONCLUSIONS

Unconfined and triaxial compression tests were conducted on Indiana limestone, Salt Wash South sandstone and Berea Buff sandstone in order to assess the effects that various fluids would have on the mechanical properties (Young's modulus, Poisson's ratio) and strength. The samples were saturated in a brine, deionized water (except for the Salt Wash South) or odorless mineral spirits. Water was found to cause the greatest reduction in strength among the fluids that were tested.

For the Indiana limestone it was discovered that the reduction in strength, via deionized water, occurs in less than 24 hours and did not significantly change when samples were saturated for a month. The cause of the weakening is believed to be stress corrosion cracking that is caused by hydrolosis groups that are chemisorbed onto fracture tips.

For Salt Wash South sandstone the presence of smectite and mixed-layer clays, as load-bearing components, suggests that clay swelling caused the dramatic reduction in strength.

For the Berea Buff sandstone it is believed that the primary weakening mechanism is similar to the primary weakening mechanism for the Indiana limestone; stress corrosion cracking. The chemical mechanism that weakens the

sandstone is caused by silanol groups that provide hydrogen ions that act as an acid at the fracture tip.

APPENDIX A

CT IMAGING OF ROCK SAMPLES

Samples were CT-scanned before testing to verify relative homogeneity and to ensure that there were no large, preexisting fractures. After testing, CT images were also taken in order to assess changes that occurred in the rock sample.

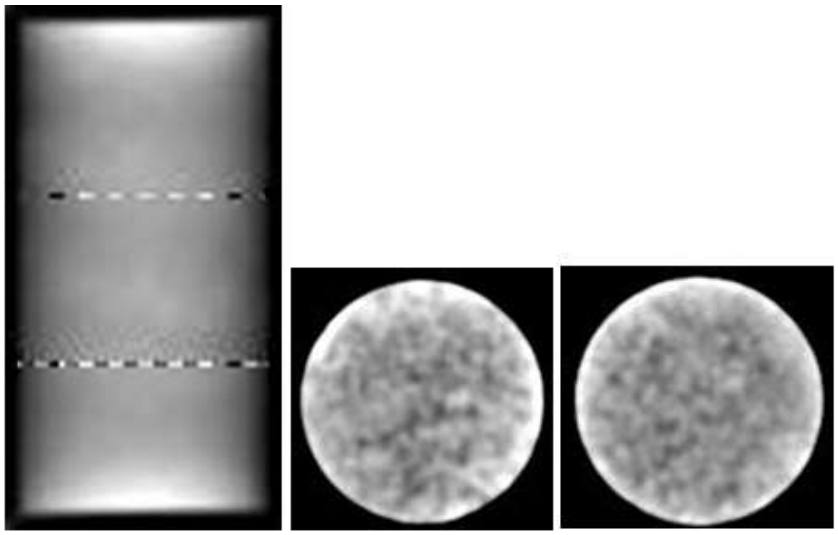

Figure 28 Sample CT image taken of an Indiana limestone plug before testing. The image on the left is a side view of the sample. The middle image is a top view and the image on the left is a bottom view. This sample appears to be fairly homogeneous and has no visible preexisting fractures.

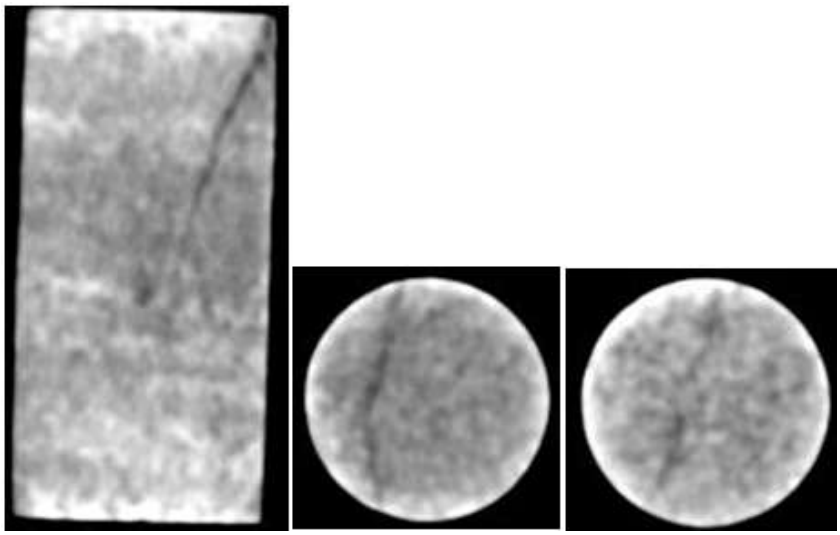

Figure 29 Sample CT image taken of the same Indiana limestone plug as Figure 28 after testing. The image on the left is a side view of the sample. The middle image is a top view and the image on the left is a bottom view. The only obvious change in the sample is the fracture that starts in the top right corner and proceeds down through the center of the sample.

APPENDIX B

INDIVIDUAL SAMPLE CHARACTERIZATION

Table 5 Diameter and length for Indiana limestone samples tested.

Sample ID	Sample Length (in)	Sample Diameter (in)
IL-1	1.99	1.00
IL-2	1.99	0.99
IL-3	1.99	0.99
IL-4	1.99	0.99
IL-5	2.00	0.99
IL-6	1.99	0.99
IL-7	1.99	0.99
IL-8	1.99	0.99
IL-9	1.99	0.99
IL-10	1.99	0.99
IL-11	1.99	0.99
IL-12	1.99	0.99
IL-13	1.99	0.99
IL-14	1.99	1.00
IL-15	2.00	0.99
IL-16	2.00	0.99
IL-17	2.00	0.99
IL-18	2.00	0.99
IL-19	2.00	0.99
IL-20	1.97	1.00
IL-21	1.97	1.00
IL-22	1.97	0.99
IL-23	1.97	1.00
IL-24	1.97	0.99
IL-25	2.00	0.99
IL-26	1.97	0.99
IL-27	1.97	1.00

Table 6 Porosity and permeability for Indiana limestone samples tested.

Sample ID	Ambient Porosity (%)	Gas Permeability (md)
IL-1	17.81	6.36
IL-2	18.94	10.49
IL-3	15.06	5.58
IL-4	15.56	4.10
IL-5	15.56	6.72
IL-6	15.32	5.66
IL-7	15.34	4.39
IL-8	15.62	6.66
IL-9	15.37	4.57
IL-10	15.72	4.68
IL-11	15.22	5.32
IL-12	17.92	7.91
IL-13	15.01	5.46
IL-14	16.30	5.79
IL-15	18.48	11.59
IL-16	15.34	6.03
IL-17	17.80	9.58
IL-18	15.26	4.65
IL-19	15.37	5.87
IL-20	16.23	4.34
IL-21	16.13	4.70
IL-22	14.96	7.04
IL-23	15.43	6.33
IL-24	15.60	5.92
IL-25	15.35	3.93
IL-26	15.80	7.13
IL-27	16.49	5.39

Table 7 Diameter and length for Salt Wash South sandstone samples tested.

Sample ID	Sample Length (in)	Sample Diameter (in)
SWS-01	2.02	1.00
SWS-02	2.02	0.97
SWS-03	2.01	0.99
SWS-04	2.02	0.99
SWS-05	2.04	0.97
SWS-06	2.03	0.97
SWS-07	2.04	0.97
SWS-08	2.01	0.96
SWS-09	2.02	0.97

Table 8 Porosity and permeability for Salt Wash South sandstone samples tested.

Sample ID	Ambient Porosity (%)	Gas Permeability (md)
SWS-01	33.43	2286.06
SWS-02	31.88	2094.25
SWS-03	32.64	2735.07
SWS-04	31.81	2295.74
SWS-05	32.65	2389.50
SWS-06	31.37	2352.27
SWS-07	32.60	2324.61
SWS-08	31.93	2663.82
SWS-09	32.63	2452.99

Table 9 Diameter and length for Berea Buff sandstone samples tested.

Sample ID	Sample Length (in)	Sample Diameter (in)
BB-1	1.96	1.00
BB-2	1.95	1.00
BB-3	1.95	1.00
BB-4	1.96	1.00
BB-5	1.95	1.00
BB-6	1.97	1.00
BB-7	1.96	1.00
BB-8	1.98	1.00
BB-9	1.97	1.00
BB-10	1.96	1.00
BB-11	1.97	1.00
BB-12	1.98	1.00
BB-13	1.96	1.00
BB-14	1.98	1.00
BB-15	1.95	1.00

Table 10 Porosity and permeability for Berea Buff sandstone samples tested.

Sample ID	Ambient Porosity (%)	Gas Permeability (md)
BB-1	21.32	279.83
BB-2	21.24	296.81
BB-3	22.54	476.42
BB-4	21.33	288.38
BB-5	21.45	295.21
BB-6	23.12	517.98
BB-7	21.18	271.40
BB-8	21.62	316.54
BB-9	23.29	615.08
BB-10	20.89	263.43
BB-11	21.64	319.69
BB-12	23.36	603.43
BB-13	21.07	269.15
BB-14	21.68	319.01
BB-15	23.29	583.21

APPENDIX C

INDIVIDUAL TEST CONDITIONS AND RESULTS

Table 11 Test conditions and results for unconfined compression testing conducted on Indiana limestone samples.

Sample ID	Saturation Fluid	Saturation Time	Peak Stress (psi)	Young's Modulus (psi)	Poisson's Ratio
IL-3	3% KCl	< 24 hours	5858	2.52E+06	0.12
IL-4	3% KCl	< 24 hours	5970	2.85E+06	0.19
IL-18	DI Water	< 24 hours	6204	2.81E+06	0.22
IL-19	DI Water	< 24 hours	6098	2.73E+06	0.18
IL-27	DI Water	< 24 hours	5714	2.88E+06	0.19
IL-20	OMS	< 24 hours	7674	3.52E+06	0.14
IL-21	OMS	< 24 hours	7691	3.69E+06	0.15
IL-22	OMS	< 24 hours	7554	3.92E+06	0.14
IL-23	Dry	N/A	8410	4.09E+06	0.17
IL-24	Dry	N/A	6920	3.22E+06	0.12
IL-25	Dry	N/A	8200	3.90E+06	0.18
IL-26	Dry	N/A	7310	3.78E+06	0.15
IL-5	DI Water	1 Week	5567	3.01E+06	0.24
IL-6	DI Water	4 Weeks	6022	3.28E+06	0.25
IL-7	DI Water	8 Weeks	6113	3.40E+06	0.20

Table 12 Test conditions and results for unconfined compression testing conducted on Salt Wash South sandstone samples.

Sample ID	Saturation Fluid	Saturation Time	Peak Stress (psi)	Young's Modulus (psi)	Poisson's Ratio
SWS-02	9% KCl	< 24 hours	48	3.00E+03	0.21
SWS-05	OMS	< 24 hours	177	1.40E+04	0.13
SWS-07	OMS	< 24 hours	168	1.30E+04	0.11
SWS-08	Dry	< 24 hours	170	1.70E+04	0.16
SWS-09	Dry	< 24 hours	203	1.90E+04	0.09

Table 13 Test conditions and results for unconfined compression testing conducted on Berea Buff sandstone samples.

Sample ID	Saturation Fluid	Saturation Time	Peak Stress (psi)	Young's Modulus (psi)	Poisson's Ratio
BB-1	Dry	N/A	5730	9.49E+05	0.18
BB-2	Dry	N/A	7840	1.06E+06	0.25
BB-3	Dry	N/A	7267	1.14E+06	-
BB-4	Dry	N/A	7152	1.11E+06	-
BB-5	Dry	N/A	6646	1.10E+06	0.29
BB-6	OMS	< 24 hours	5334	1.09E+06	0.30
BB-7	OMS	< 24 hours	5999	1.10E+06	0.37
BB-8	OMS	< 24 hours	6618	6.40E+05	0.24
BB-9	OMS	< 24 hours	6352	1.12E+06	0.27
BB-10	OMS	< 24 hours	5479	8.86E+05	0.23
BB-11	OMS	< 24 hours	7375	1.21E+06	0.29
BB-12	H2O	< 24 hours	6352	1.12E+06	0.31
BB-13	H2O	< 24 hours	5162	1.00E+06	0.23
BB-14	H2O	< 24 hours	5304	1.09E+06	0.31

BIBLIOGRAPHY

Al-Tahini, A. M., Sondergeld, C. H., and Rai, C. S. 2003. The Effect of Cementation on the Mechanical Properties of Sandstones. Master of Science thesis, University of Oklahoma, Norman, Oklahoma.

Ashby, M. F. 1972. A first report on deformation mechanism maps. *Acta Metallurgica* **20** (7): 887-897.

Atkins, B., and Meredith, P. 1981. Stress corrosion cracking of quartz: a note on the influence of chemical environment. *Tectonophysics* **77** (1): T1-T11.

Atkinson, B. 1979. A Fracture Mecahnics Study of Subcritical Tensile Cracking of Quartz in Wet Environments. *Pure and Applied Geophysics* **117**: 1011-1024.

Atkinson, B. 1980. Stress Corrosion and the Rate-Dependent Tensile Failure of a Fine Grained Quartz Rock. *Tectonophysics* **65** (3): 281-290.

Atkinson, B. and Meredith, P. 1984. Fracture toughness and subcritical crack growth during high-temperature tensile deformation of Westerly granite and Black gabbro*. Physics of The Earth and Planetary Interiors* **39** (1): 33-51.

Austin, N. and Evans, B. 2009. The kinetics of microstructural evolution during deformation of calcite. *Journal of Geophysical Research* **114** (1): 1-22. doi:10.1029/2008JB006138.

Clementz, D. 1977. Clay Stabilization in Sandstones Through Adsorption of Petroleum Heavy Ends. *Journal of Petroleum Technology* **29** (9): 1061-1066. SPE-6217-PA. doi: 10.2118/6217-PA

Colback, P. S., and Wiid, B. L. 1965. The influence of moisture content on the compressive strength of rock. Oral presentation given at the 3rd Canadian Symposium on Rock Mechanics, Toronto, Canada .

Hawkins, A. B. and McConnell, J. 1992. Sensitivity of sandstone strength and deformability to changes in moisture content. *Quartlerly Journal of Engineering Geology* **25** (2): 115-130.

Ulusay, R. H. ed. 2007. *The Complete ISRM Suggested Methods for Rock Characterisation, Testing and Monitoring.* Ankara: International Society for Rock Mechanics.

Le Guen, Y., Renard, F., Hellmann, R., Brosse, E., Collombet, M., and Tisserand, D. 2007. Enhanced deformation of limestone and sandstone in the presencse of high pressure CO2 fluids. *Journal of Geophysical Research* **112** (1), 1-21. doi: 10.1029/2006JB004637.

Mohamed, F. A., & Landgdon, T. G. 1974. Deformation Maps Based on Grain Size. *Metallurgical and Materials Transactions* **5**: 2339-2345.

Rutter, E. H. 1983. Pressure soluiton in nature, theory and experiment. *Journal of the Gelolgical Society* **140** (5): 725-740. doi: 10.1144/gsjgs.140.5.0725.

Rutter, E. H., & Elliot, D. (1976). The kinetics of rock deformation by pressure solution. *Philosophical Transactions of the Royal Society of London. Series A. Mathematical and Physical Sciences* **283** (1312): 203-219. doi: 10.1098/rsta.1976.0079.

Stipp, S. L. 1999. Toward a conceptual model of the calcite surface: Hydration, hydrolysis, and surface potential. *Geochimica et Cosmochimica Acta* **63** (19): 3121-3131. doi: 10.1016/S0016-7037(99)00239-2.

Tomkins. B., Grover, H. K., Grey, T. 1981. Subcritical crack growth: Fatigue, creep and stress corrosion cracking. *Pilosophical Transactions of the Royal society of London. Series A. Mathematical and Physical Sciences* **299** (1446): 31-44. doi: 10.1098/rsta.1981.0007.

Vutukuri, V. S., Lama, R. D., and Saluja, S. S. 1974. *Handbook on Mechanical Properties of Rock, Volume I.* Clausthal: Trans Tech Publications.

Wiederhorn, S. M. 1978. Subcritical crack growth in ceramics. *Fracture Mechanics of Ceramics* **4** (1): 613-646.